Construction and Building Materials 391 (2023) 131806

Contents lists available at ScienceDirect

Construction and Building Materials

journal homepage: www.elsevier.com/locate/conbuildmat

The effect of PVA microfiber reinforcement on the mechanical and rheological behavior of class G oil well cement pastes

Victor Nogueira Lima [a,c], Hans Joakim Skadsem [b,c,*], Katherine Beltrán-Jiménez [c], Raquel Quadros Velloso [a], Flávio de Andrade Silva [a]

[a] Department of Civil and Environmental Engineering, Pontifícia Universidade Católica do Rio de Janeiro (PUC-Rio), Rua Marquês de São Vicente 225, 22451-900 Rio de Janeiro, Brazil
[b] University of Stavanger, P.O. Box 8600, 4036 Stavanger, Norway
[c] Norwegian Research Centre AS, P.O. Box 8046, 4068 Stavanger, Norway

ARTICLE INFO

Keywords:
Cement
PVA fiber
Rheology
Early age
Mechanical properties
Well cementing

ABSTRACT

During the life cycle of an oil well, the annular cement sheath will be exposed to load combinations that can result in failure. To enhance the structural integrity and ductility of the cement paste, and to improve the resistance to tensile crack propagation, fiber reinforcement can be used. In the present work, the effects of different polyvinyl alcohol (PVA) fiber concentrations on the rheological and mechanical properties of a class G oil well cement paste was investigated. The study focuses on impacts of fibers on the cement paste viscosity, its confined and unconfined stress–strain responses, and resistance to shear and bending loads. An increase in the effective viscosity of the cement paste with increasing fiber content was observed, although the impact was minor for the smallest (semi-dilute) fiber concentration. All cement paste specimens showed a modest frictional strengthening with increasing confining pressure, with the fiber reinforced samples exhibiting improved post-peak load-bearing capacity compared to the base formulation with no fiber additive. Fibers were found to significantly improve cement paste resistance to shear and bending loads, to enhance the toughness and to arrest tensile crack growth. Despite all the benefits already known about adding fibers, for application in the oil and gas industry, it is essential to evaluate the rheology of the mixture that will directly impact pumpability and placement. In this work, flow curves were measured only for concentrations ranging from 0.1% to 0.5% since the other cases approached the concentrated suspension regime with the fluid behaving like a plug. Still, the results elucidate the potential benefits of adding even a relatively small concentration of high-aspect-ratio PVA fibers to oil well cement pastes, particularly for enhancing early-age cement's shear and bending strength.

1. Introduction

Oil well cement paste is by far the most widely used material for achieving zonal isolation in wells, both for primary cementing of casing strings during well construction, and for reestablishing natural barriers as part of well abandonment. Annular cement sheaths and permanent cement plugs are exposed to different load combinations, such as hydrostatic pressure variations, fluid injection operations, or mechanical loads due to pressurization of the well or due to casing expansion [1]. In particular, tensile stresses in the annular cement sheath can be caused by radial casing expansion (*e.g.* due to pressure, thermal or mechanical loading of the casing) in cases where the cement sheath is not firmly supported by an outer casing or the surrounding rock formation. As cements are typically weak in tension, such loads can cause tensile failure and cracks through the cement [1]. Increasing the tensile strength of the cement while reducing its modulus of elasticity can increase the robustness toward tensile failure. Therefore, there is a need to develop oil well cement paste compositions that are highly resilient and flexible to withstand downhole stresses. The purpose of the present study is to investigate the potential impacts of adding different concentrations of polyvinyl alcohol (PVA) fibers to a conventional class G oil well cement paste, with a particular emphasis on the viscosity and mechanical properties of the fiber-reinforced cement paste.

Cement-based composites were developed a few decades ago to be used in applications where post-peak residual strength is required to provide ductility and toughness to the material [2–7]. Fiber-reinforced cementitious materials have been found to improve the ductility of the materials when subjected to increasing tensile stresses [8,9], and

* Corresponding author at: University of Stavanger, P.O. Box 8600, 4036 Stavanger, Norway.
E-mail address: hans.j.skadsem@uis.no (H.J. Skadsem).

https://doi.org/10.1016/j.conbuildmat.2023.131806
Received 2 February 2023; Received in revised form 11 April 2023; Accepted 13 May 2023
Available online 23 May 2023

also to improve the durability of materials when subjected to severe environmental conditions [10–13]. Several studies have addressed the behavior of cementitious composites when subjected to direct tensile and bending loads [11,14–18]. Considering studies that use short fibers to reinforce cement pastes and mortars, van Zijl investigated the behavior of strain hardening cementitious composites (SHCC) reinforced with PVA fibers [19]. The study showed that SHCC composites present strain-hardening behavior when subjected to shear loads, as observed in the case of direct tensile tests. In the same study, it was also observed that the ultimate shear strength was approximately 50% larger than the direct tensile strength, which may be explained by the growth of orthogonal compressive stresses. The use of PVA fibers to reinforce cementitious materials subjected to shear stresses was also recently evaluated by Baghi and Barros using the Iosipescu test which is traditionally adopted for polymeric composites [20] . According to this study, the applied stress and apparent crack sliding behavior of the composite may be divided into three phases. First, a brief linear phase was observed, which was likely controlled by the deformation of the matrix. A slip-hardening phase followed, where the cracking pattern of the sample developed. Finally, a slip-softening phase was observed that was now governed by the opening of existing cracks, the formation of macro-cracks and a reduction of the material strength.

The inclusion of fibers in cement pastes for oil well applications was recently explored by Yang and Deng using polyester fibers and calcium carbonate whisker [21]. The study showed that addition of polyester fiber increased the flexural and tensile strengths by 19.4% and 40.1%, respectively, while the compressive strength was reduced by 11.5%. In confined compression tests, the plastic behavior of the material and the peak stress were larger for the fiber-reinforced cement paste, which resulted in a ductile behavior in the stress–strain curve. In addition, the study showed that the absorbed energy and compressive toughness of fiber-reinforced cement pastes increased compared to pastes without fiber additive [21]. These observations indicate that fiber reinforcement brings advantages to oil well cement in the form of high deformation capacity and significant energy absorption in the post-peak zone.

Several studies have investigated the mechanical properties of fiber reinforced cementitious composites under downhole conditions and with different fiber reinforcements. Serafini et al. evaluated the bond–slip behavior of steel fibers after submitting the samples to different curing temperatures, ranging from 25 °C to 750 °C, [22]. They observed that for temperatures up to 450 °C there was a significant improvement in bond strength, but it reduced dramatically for temperatures above 600 °C. Furthermore, the study suggested that the increase in bond strength could be associated with changes in the Si/Ca ratio, which in turn alters the structure of the interfacial transition zone (ITZ). Changes in ITZ can result in increased interfacial chemical adhesion and increased dynamic frictional interaction between fiber and matrix due to densification. In the case of PVA fiber, the bond–slip behavior of the fiber subjected to high temperature is significantly affected by the polymer degradation process. Li et al. studied the effect of temperature on PVA fiber morphology, and they showed that changes in the molecular structure of the polymer chain occur due to oxidation reactions at temperatures up to 200 °C, [23]. This molecular change was also found by Li et al. [24]. Through thermal analysis of PVA fibers, Du et al. found that the onset of thermal PVA fiber degradation occurs at temperatures of approximately 100 °C, although impacts on the mechanical behavior was also observed at lower temperatures [25]. Further Magalhães et al. evaluated the behavior of SHCC specimens reinforced with PVA fibers [26]. Their study demonstrated a slight alteration to the residual tensile strength response when testing at 90 °C, and that toughness and crack density are reduced compared to unheated specimens due to changes in fiber microstructure.

While the above discussion has mostly focused on fiber additive impact on the mechanical properties of cementitious materials, and their positive influence on the toughness, tensile strength and improved resistance to bending stresses and crack propagation, fibers are also expected to affect the viscosity of the cement paste during mixing and placement [27,28]. The importance of cement paste viscosity is linked to cement placement (and mud displacement), and should be considered as part of cement paste design. The effect of fibers on fluid viscosity is connected to the degree of fiber particle interactions, which in turn motivates the distinction between dilute, semi-dilute and concentrated fiber suspensions. Many commercially available fibers are typically long and slender, with a large length-to-diameter (aspect ratio, $a = l/d$). Unless exceedingly small fiber concentrations are used, high-aspect ratio fibers will be prevented from rotating completely freely in the fluid due to the large volume they span out as they rotate. At volume fractions of approximately a^{-1} or greater, the interaction between neighboring fibers in the fluid will significantly constrain their rotation and orientation, [27]. For the PVA fiber which is subject to this study, $a \approx 222$, suggesting considerable constraints on the alignment of individual particles at volume concentrations of 0.5% and higher. Indeed, when high-aspect ratio fibers are used as additive in wellbore clean-out fluids, fiber concentrations even less than 0.1% are found highly effective in improving hole cleaning in deviated wellbores [29].

As suggested by the literature review above, fiber reinforcement of cementitious materials is expected to improve the toughness, ductility and post-peak behavior of the material. Enhancing these properties of oil well cements can bring about a more robust downhole barrier that may be used in combination with *e.g.* an expanding additive to make a durable barrier for zonal isolation. The purpose of this study is to investigate the impact of different concentrations of a PVA fiber on the viscosity, that impacts pumpability and placement, and the early-age mechanical properties of a class G well cement.

Table 1
The oxides from the class G oil well cement used with the requirements of the API 10A standard (2011).

Chemical property	Value	Requirement
SiO_2, %	22.30	N/A
Al_2O_3, %	3.88	N/A
Fe_2O_3, %	4.52	N/A
SO_3, %	2.39	<3%
CaO, %	64.54	N/A
MgO, %	1.46	< 6%
Na_2O, %	0.55	<0.75%
K_2O, %	0.36	N/A

2. Material design and mixing protocol

For this study, an oil well class G cement paste with nominal strength of 45 MPa after 28 days was developed and stabilized. In the design of the cement paste, fluid loss and defoamer additives were included to control loss of filtrate and to mitigate the surfactant effect of the fluid loss additive. The chemical composition of the class G cement that was used for the study, highlighting the main oxides present, is shown in Table 1. This class G cement has a Blane fineness of 2854 cm^2/g and a mass density of 3.19 g/cm^3. Deionized water was used in the process of mixing the cement paste considering the water/cement ratio of 0.44 defined by the API 10 A [30] and API 10B [31] standards for the class G cement. Quality control tests were carried out on the mixture without additives, following the recommendations of API 10 A standard, *e.g.* free water test, thickening time test, and compressive strength test after 8 h curing. Table 2 summarizes the results for the cement quality control tests.

The two additives used in this study was a powder polyvinyl alcohol (PVOH) fluid loss additive with viscosity 49 mPa·s, a degree of hydrolysis of 88%, and granulometry between 0.063 mm and 0.25 mm. A commercial liquid defoamer additive (Basopur DF5) based on fatty alcohol alkoxylate, and produced by BASF, was also used. The final base cement paste composition is presented in Table 3. As fiber additive for reinforced cement paste samples, the Kuralon RMS702 PVA fiber

Table 2
Cement quality test results for class G cement paste according to API 10 A specification.

API 10A test	Value	Requirement
Water/cement ratio	0.44	0.44
Free water	4.71%	< 5.90%
UCS, cured at 38 °C	5.6 MPa	> 2.1 MPa
UCS, cured at 60 °C	13.7 MPa	> 10.3 MPa
Thickening time, 30 Bc	70 min	> 30 min
Thickening time, 70 Bc	98 min	N/A
Thickening time, 100 Bc	107 min	90–120 min

Table 3
Class G cement paste mixture compositions.

Material	Manufacturer	Mix proportion
Class G cement	Lafarge Holcim	0.44 w/c ratio
Deionized water	–	
Fluid loss additive	Kuraray	0.4% bwoc[a]
Deforamer	BASF	0.1% bwoc[a]
PVA fiber	Kuraray	0.5%, 1.0%, 1.5%[b]

[a]bwoc: by weight of cement.
[b]by total volume.

Table 4
PVA fiber properties according to the manufacturer Kuraray.

Property	Value
Diameter (μm)	27
Length (mm)	6
Aspect ratio	222
Density (g/cm^3)	1.3
Tensile strength (MPa)	1600
Elongation (%)	6
Young's modulus (GPa)	37

produced by Kuraray, was used. The properties of the PVA fiber are shown in Table 4. Other polymeric fibers could have been chosen, but PVA fibers present better bond strength when compared to the others, ranging from 0.81 to 2.44 MPa [32–34], and, therefore, can result in a significant improvement in mechanical behavior even using low fiber contents.

The cement paste mixing process consisted of two stages, the first being the mixing of the cement paste base formula, and the second stage being the dispersal of fibers when producing the reinforced samples. For the first stage, a constant speed Chandler model 3260 mixer was used to mix the materials in accordance with the API standard and using the following sequence: Add water and liquid additives to the mixing container; manual mixing of cement and powder additives in a separate container; add the dry ingredients to the liquid mixture while mixing at a constant speed of 4,000 revolutions per minute (RPM) for 15 s; mix for another 35 s at a constant speed of 12,000 RPM. The reference samples were molded after this step, while the composites went through another mixing process to disperse the fibers in an IKA model EUROSTAR 60 mixer. In this last step, the fibers were added to the cement paste over an interval of 1 min and then allowed to disperse for another 4 min at a constant speed of 500 RPM.

The experimental characterization and testing of the fiber reinforced cement pastes include viscosity measurement, unconfined and confined compression strength test, and early age mechanical tests, such as Iosipescu shear strength test and three-point bending test. Regarding the curing procedure, all early-age samples were allowed to cure for three days submerged in water at room temperature of 27 °C. Only a group of samples from the bending test were allowed to cure in a thermal bath at an average temperature of 70 °C, to evaluate the effect of the curing temperature on the ability of the PVA fiber to control crack openings. On the third day, the specimens were removed from the water and allowed to dry in order to apply the Digital Image Correlation (DIC) speckles on their surface. Specimens for the triaxial tests were cured for 28 days at room temperature and atmospheric pressure, ensuring a decrease in the influence of the hydration process and material strength development on the compressive stress–strain behavior. Finally, samples for viscosity measurements were collected and tested immediately after the mixing procedure. An overview of the test program is provided in Fig. 1.

3. Experimental test program

3.1. Rheology

A Fann 35 rotary viscometer was used to measure the viscosity of the cement paste with and without the addition of PVA fibers. In an effort to minimize the impact of the measurement geometry on the fiber orientation, a wide gap (R1-B2) measurement cell was used to measure the viscosity of the cement paste samples containing fibers. This measurement cell consists of an outer rotor (R1) of radius 18.415 mm and an inner stator (B2) of radius 12.276 mm, which produces a measurement gap width of 6.139 mm wide. The reference cement slurry without fiber additive has been measured in both the wide gap geometry, and in the standard narrow gap geometry (R1-B1), using the same rotor and an inner stator of radius of 17.245 mm. In all cases, the viscosity has been measured using rotational speeds of 3, 6, 30, 60, 100, 200, and 300 revolutions per minute.

As the cement paste was expected to be shear thinning and potentially exhibit a minor yield stress, non-Newtonian effects was accounted for when assessing the wall shear rate at the bob and the shear stress end-effects [35,36].

3.2. Uniaxial and triaxial compression tests

The impact of fibers on unconfined (uniaxial) and confined (triaxial) compressive strength of the cement paste was studied using cylindrical samples of 50 mm diameter and 100 mm height. The compression tests were performed with an MTS model 815 machine equipped with an MTS flex test 60 controller, and with one circumferential strain gauge and two axial strain gauges, as seen in Fig. 2. These gauges were used both for measuring the strain during the test, and for controlling the machine: Uniaxial compression tests were performed by loading the specimens at a circumferential strain rate of $5{\cdot}10^{-5}$ s^{-1} until failure was detected. Consequently, since circumferential strain control allowed samples to fail in a controlled manner, this also enabled sampling of the post-peak behavior. Triaxial testing were performed with either 10 MPa or 20 MPa confining pressures. The triaxial test cell was filled with Mobil Mobiltherm 605 oil and confining pressure was applied by hydrostatically loading the sample at a rate of 2 MPa/min until reaching target confining pressure. The deviatoric loading phase was performed as per the uniaxial tests. All specimens underwent a rigorous preparation process, using self-fusing silicone tape and a heat-shrinkable fluorinated ethylene propylene (FEP) membrane, as already described by Lima et al. [37] and Lorenzoni et al. [38]. Repeatability was controlled by repeating each test with three separate specimens.

3.3. Shear and bending tests

To further assess the potential impact of fiber addition on the mechanical performance of well cements, additional shear and bending tests were performed using cement samples cured for 3 days (early-age samples). The Iosipescu shear test was performed to measure shear strain and crack sliding as function of applied shear stress, and was implemented in accordance with ASTM 5379/5379 M [39]. The experimental setup is shown in Fig. 3. A universal testing machine with an MTS servo-hydraulic actuator model 810, a 500 kN loading capacity, and one servo-valve was used to perform the tests. The tests were conducted with a closed-loop system using displacement control, ensuring a constant displacement rate of 0.1 mm/min. The apparent sliding of the crack was measured with the aid of an external linear

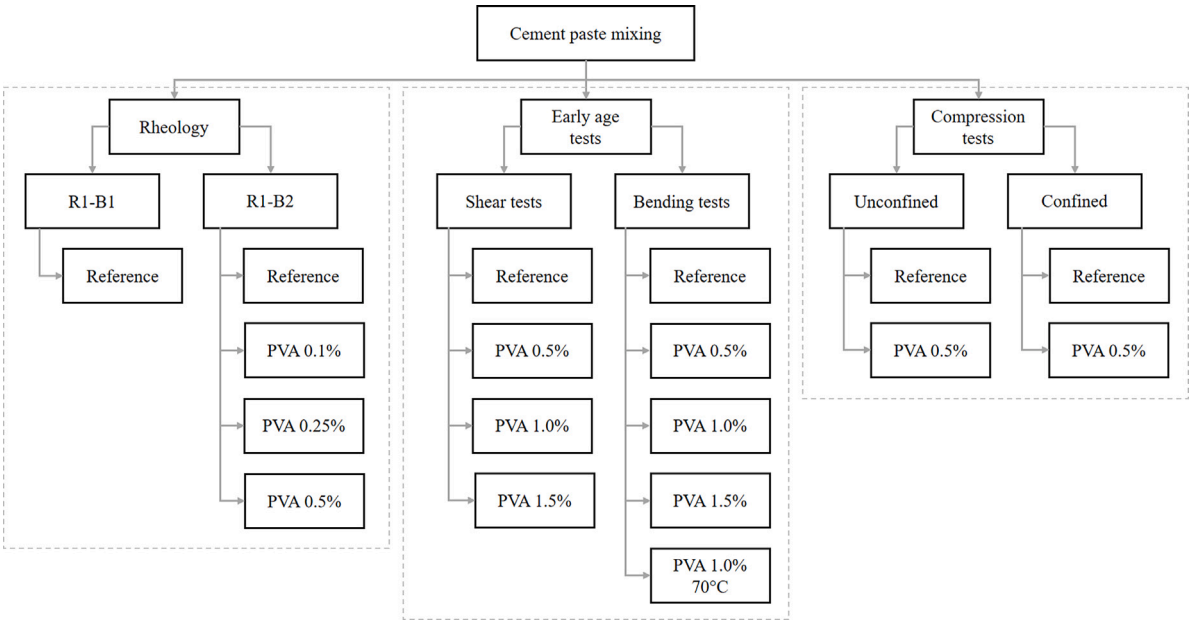

Fig. 1. Experimental program summarized in flowchart.

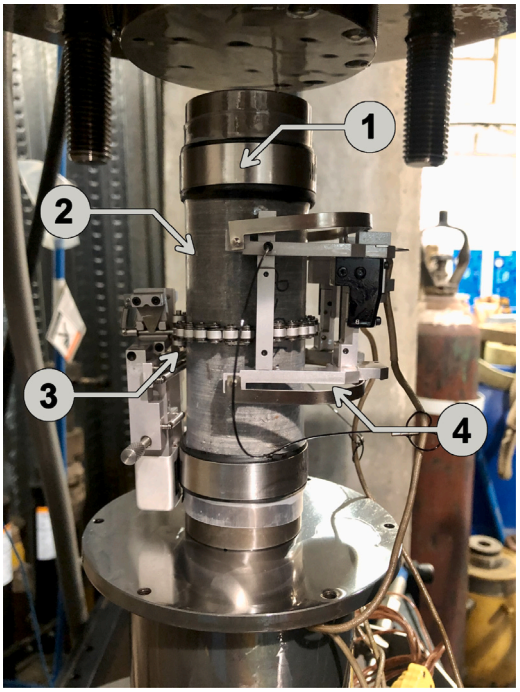

Fig. 2. Compression test setup. (1) is the cylindrical specimen with self-fusing silicone electrical tape, (2) is the heat shrinkable FEP membrane (Roll CoverHeat Shrink® from Zeus™), and finally the specimen positioned in the MTS triaxial testing machine with the circumferential clip gauge (3) and the axial LVDT (4).

variable displacement transformer (LVDT), and the strains in the shear region were acquired through a pair of strain gauges positioned at ±45° in the direction of the notch. This experimental arrangement has been used in other recent research involving cementitious materials, and we refer to Teixeira et al. [40] and Lorenzoni et al. [41] for more details. The crack pattern was analyzed with the help of digital image correlation (DIC), which is a method that correlates the displacement of the speckle pattern on the surface of the sample by comparison against the reference image [42,43]. To capture the images, a Canon T6 rebel camera externally controlled by the computer was used at a rate of 0.1 Hz. Finally, the GOM Correlate software was used to analyze the captured images, adopting subsets of 25 pixels.

Next, three-point bending tests were performed on notched specimens using the same MTS servo-hydraulic actuator model 810, as described above. Three specimens were produced for each cement paste mix, with cross section of 40 mm × 40 mm, length of 160 mm and notch of 10 mm in depth and 2 mm wide. A three-point bending configuration was used, with a 150 mm span between end supports, as shown in Fig. 4. The tests were controlled by the crack mouth opening displacement (CMOD) using an MTS clip-gauge model 632.02B-20 limited to 4 mm opening. The CMOD was adopted as a test displacement controller under a constant rate of 0.05 mm/min up to a CMOD of 0.1 mm. From then on, the CMOD rate was changed to 0.20 mm/min until the crack mouth opening reached 4 mm. DIC analysis was performed using the same setup as for the Iosipescu shear strength tests described above. We refer to Tinoco and Silva [44] and Bareiro et al. [6] for additional details concerning the test equipment and procedures.

4. Results and discussion

4.1. Rheology

As discussed above, a wide-gap Couette measurement geometry (R1-B2) was utilized for measuring the viscosity of cement paste samples with fiber additive. To verify the calibration of the viscometer, the viscosity of the reference cement paste without fiber additive was measured using both the narrow gap (R1-B1) and the wide gap (R1-B2) measurement geometry. Shown in Fig. 5(a) as open symbols are measurements acquired using the conventional numerical (Newtonian) conversion factors for converting torque and rotational speed to shear stress and shear rate at the bob. Comparing the two measurement series shown with open symbols, one observes that measurements acquired with the wide gap (R1-B2) geometry appears to suggest a more viscous slurry than the measurements obtained using the narrow gap geometry (R1-B1). However, when correcting for the non-Newtonian end effects on the inner bob, and the non-Newtonian shear rate in the gap, as shown by the filled symbols, an excellent agreement is achieved for the flow curve. Due to the wider gap in R1-B2, lower wall shear rates are realized at the given rotational speeds, but the resulting flow curves are in excellent agreement where they overlap in wall shear rate.

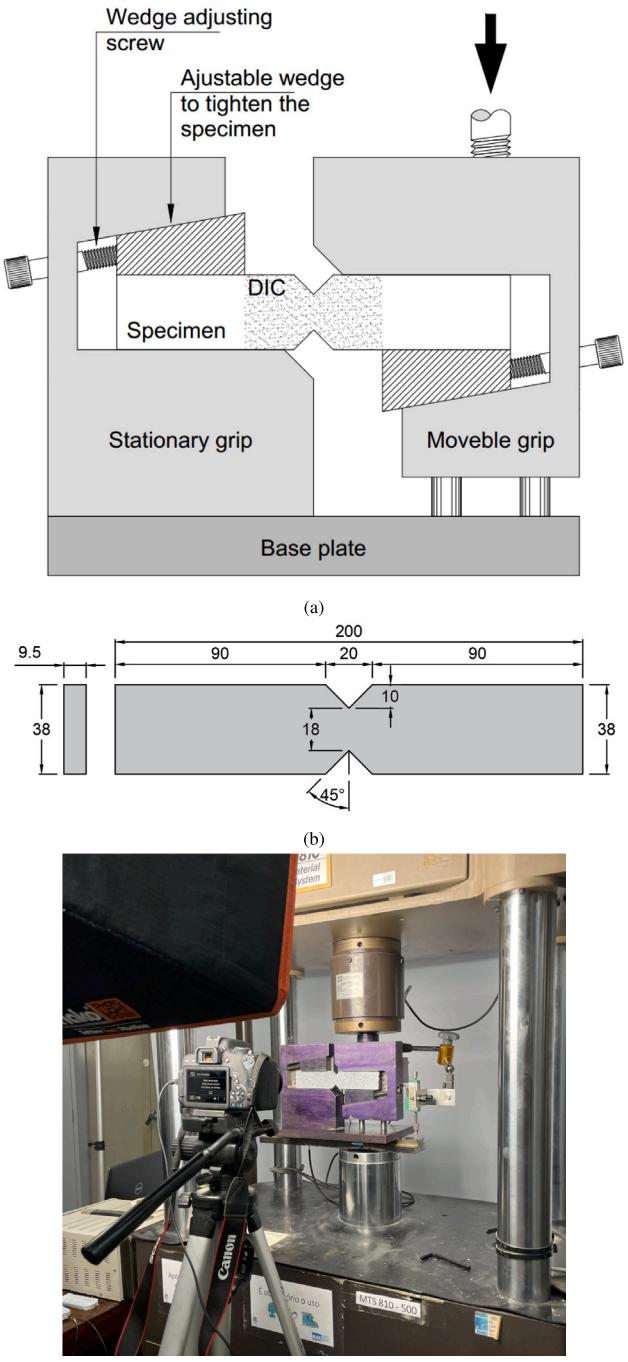

Fig. 3. The Iosipescu test scheme (a), specimen geometry (b), and Iosipescu shear test setup (c). All dimensions in mm.

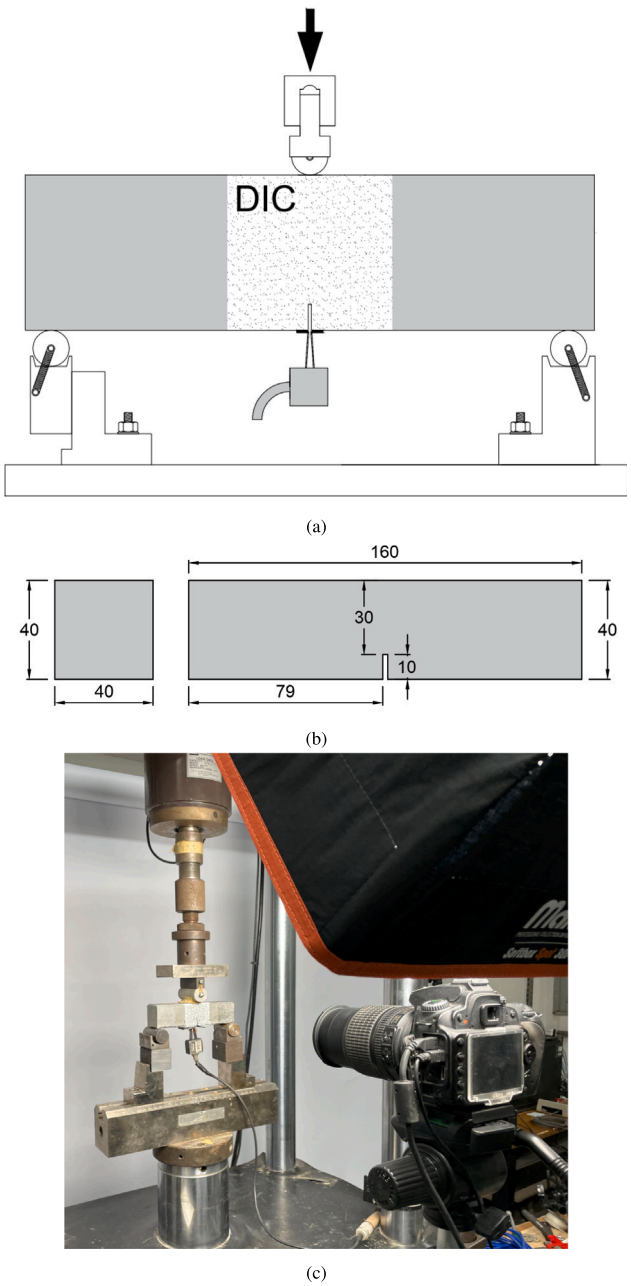

Fig. 4. The three-point bending test scheme (a), specimen geometry (b), and bending test setup (c). All dimensions in mm.

In Fig. 5(b), corresponding flow curves are shown for the cement pastes with varying concentration of fiber additive. Only the wide gap measurement geometry is used for samples containing fiber, in order to limit the orientational confinement of individual fiber samples inside the measurement gap. As anticipated, the flow curves shown in Fig. 5(b) suggest an increasing effective viscosity with increasing fiber content in the sample. The solid lines in the figure correspond to least squares fits of the measurements to the Herschel–Bulkley constitutive model, $\tau = \tau_y + K\dot{\gamma}^n$, where τ and $\dot{\gamma}$ are the shear stress and shear rate at the wall of the stator, respectively, and τ_y, K and n are model parameters referred to as yield stress, consistency index and flow index, respectively. A listing of the least squares fitted model parameters is provided in Table 5 for all formulations tested.

All samples are seen to exhibit yield stress behavior with $\tau_y \approx 3-5$ Pa. Increasing fiber concentration is seen to induce a significant shear thinning behavior, as evident from the combination of consistency index and flow index at the two largest concentrations of fiber additive. We consider these observations for the high-aspect ratio PVA fiber to be in qualitative agreement with Martinie et al. [28], where it was found that the impact of fibers on the viscosity of cementitious materials should be limited for fiber volume fractions considerably smaller than $3.2/r$, where r is the fiber aspect ratio, *i.e.* the ratio of fiber diameter to length. For the values in Table 4, PVA fibers have a nominal $r \approx 222$, which suggests limited impact of fiber additive on the suspension viscosity for volume fractions $\ll 1.4\%$.

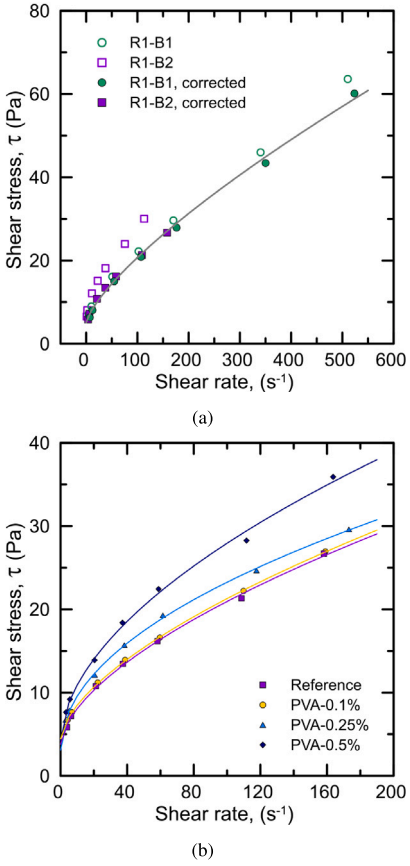

Fig. 5. (a) Flow curves for the reference cement paste (no fiber additive) using the narrow gap (R1-B1) and wide gap (R1-B2) viscometer measurement geometries. (b) Flow curves for cement paste with varying fiber content using the wide gap geometry.

Table 5
Herschel–Bulkley model parameters for each sample tested.

Formulation	τ_y (Pa)	K (Pa s^n)	n
Reference	5.13	0.50	0.75
PVA-0.1%	4.46	0.97	0.62
PVA-0.25%	3.10	2.09	0.49
PVA-0.5%	4.23	1.88	0.55

4.2. Uniaxial and triaxial compressive strength of cement samples

Results from the unconfined and the confined compression tests are shown in Fig. 6 in the form of stress–strain curves. In this figure, and in the remainder of the paper, compressive stresses and strains are taken as positive and the lateral (extensional) strain is taken as negative. Stress–strain curves are here shown for the reference cement paste without fibers, and for samples with 0.5% fiber addition. For the unconfined compression tests, we observe similar maximum deviatoric stresses across these samples and little to no significant impact on the stress–strain curves due to fiber addition. The maximum deviatoric stresses reach values of approximately 60 MPa, independent of fiber content. A transition from linear to slight non-linear behavior was observed at an axial strain of approximately 0.2%, followed by brittle response after the peak stress. The reference samples containing no fiber additive exhibited an abrupt loss of load-carrying capacity. A certain residual strength was observed in samples reinforced with 0.5% PVA fiber additive. This is likely linked to fiber particles bridging internal shear cracks in the cement specimens before macroscopic failure.

In the case of samples tested under confining pressure, the stress–strain responses exhibited significant ductile behavior in all samples tested. This observation is in line with previous studies, such as [45–47]. Compared to the unconfined samples that failed at an axial strain of approximately 0.55%, the confined reference samples were able to achieve 1% axial strain without losing load-carrying capacity. On the other hand, PVA 0.5% samples showed a prolonged plastic phase, apparently without loss of load-carrying capacity until the end of the test. Furthermore, both cement pastes showed modest reinforcement by friction with increasing confining pressure. This frictional reinforcement is more evident in the sample reinforced with 0.5% PVA fiber. However, since only two formulations were tested at two confining pressures, additional future tests should be performed to identify systematic trends related to level of confining pressure or fiber concentration.

Table 6
Summarized composite properties by mechanical analysis under three-point bending load.

Formulation	Confining pressure	E (GPa)	ν
Reference	0 MPa	16.57 ± 0.60	0.14 ± 0.01
	10 MPa	15.66 ± 0.48	0.10 ± 0.01
	20 MPa	14.88 ± 0.27	0.09 ± 0.01
PVA-0.5%	0 MPa	16.86 ± 0.75	0.14 ± 0.01
	10 MPa	15.44 ± 0.10	0.09 ± 0.01
	20 MPa	15.34 ± 0.43	0.09 ± 0.01

Fig. 7 shows the measured volumetric and axial strains for the cement samples. Here, the volumetric strain is taken as $\varepsilon_{vol} = \varepsilon_z + 2\varepsilon_x$, where ε_z and ε_x are the axial and lateral strains, respectively. We note that the samples underwent volumetric compression during most of the loading. However, two of the reference samples submitted to 10 MPa of confinement showed dilating trends prior to failure, suggestive of internal crack propagation.

Finally, since $\varepsilon_{vol} = (1 - 2\nu)\varepsilon_z$ for elastically deformed materials, the Poisson ratio can be estimated from the linear part of these strain curves. Values for Young's modulus and the Poisson ratio obtained from the initial linear stress–strain curve are shown in Table 6. When comparing the reference formulation to the formulation with fiber additive, we find values that are not significantly different, as indicated by the error margins in the table. Thus, fiber addition does not influence the linear elastic behavior of the cement specimens, nor the maximum deviatoric stress level, as seen from Fig. 6. The main difference in the stress–strain behavior of the specimens, is considered to be the increased ductility and post-peak load-carrying capacity of cement samples with fiber addition. Finally, we note that increasing confining pressure results in decreasing values of the Young's modulus and the Poisson's ratio for all samples considered, similar to previous measurements for a comparable oil well cement slurry under the same confining pressure, [37].

4.3. Shear strength

While the fiber additive exerted relatively modest impacts on the viscosity and the compressive stress–strain behavior of the cement paste, a more significant impact is expected for the shear and flexural strength of the specimens. We now examine results from the Iosipescu shear strength tests, and show in Fig. 8(a) the shear stress plotted as function of apparent crack sliding for all cement paste mixtures. For each group of specimens tested, the results showed similar shear strength and crack sliding. When evaluating the fiber increment in the mixture, it can be seen that not only the maximum shear stress increased but also the apparent crack sliding value at the peak stress, as seen in Table 7. Therefore, in addition to increasing the shear strength of the material, its ductility is also enhanced. Furthermore, the graph of Fig. 8(b) shows the relationship between the stress and the strain measured by the pair of strain gauges, where the strain is calculated as the sum of the strain gauges absolute readings. For this plot, only the

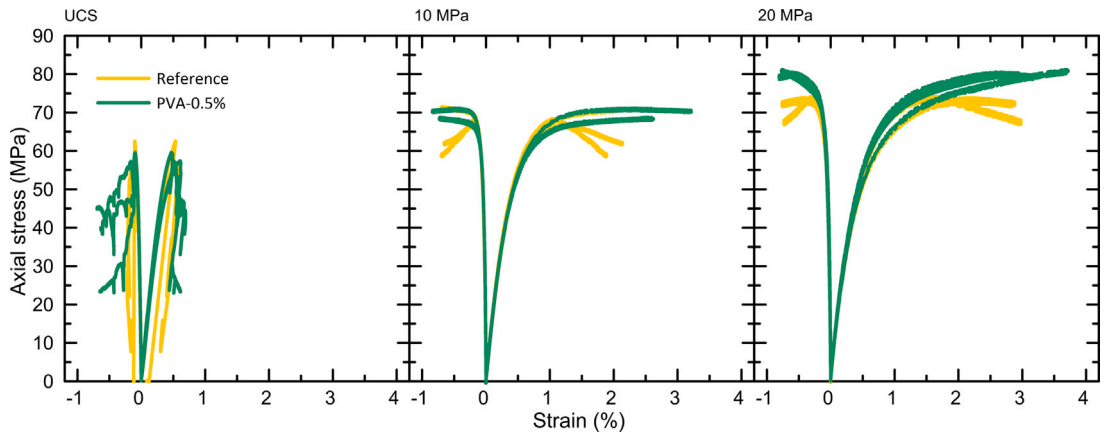

Fig. 6. Measurements of axial and lateral strains for increasing deviatoric stresses at unconfined conditions (UCS) and at two different confining pressures.

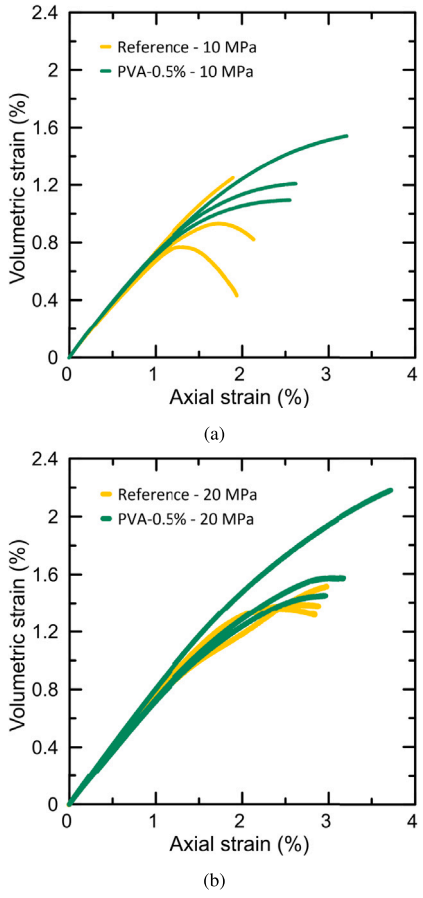

Fig. 7. Axial and volumetric strains measured at different confining pressures and for the two formulations. (a) The results for 10 MPa confining pressure and (b) for 20 MPa. The volumetric strain is measured relative to the start of the deviatoric loading phase.

average curve for each mixture was presented due to the variability of the readings.

In Fig. 8(c) we compare our measurements to recent tests performed on fiber-reinforced cementitious composites: Teixeira et al. [40] reported results for a *curauá* natural fiber additive, while Baghi and Barros [20] studied a strain hardening cementitious composite (SHCC) reinforced with 2% of discrete PVA fibers. We note that the matrices of the two samples used for comparison purposes were significantly different from the class G cement paste matrix utilized in the current study, since fine aggregate and mineral additions are utilized in their compositions. Moreover, cementitious matrices used for the formulation of SHCC materials have fine control of the granulometry of their constituents, which improves the material performance [2,32,48]. Therefore, the difference observed in Fig. 8(c) for the initial behavior of the stress by crack sliding curves may be linked to the different material matrices. Curing time may also partly explain the variations, since the samples in this research are *early age* samples, tested after merely three days of curing. However, it can be seen that from the moment the fiber starts to play its role of bridging the cracks and redistributing the stresses, the hardening behavior found in the other samples becomes evident for the class G cement paste matrix mixtures.

Table 7 summarizes the mechanical properties and cracks pattern for the PVA fiber-reinforced class G cement paste. The crack opening and number of cracks described in Table 7 was measured by the DIC performed for each specimen. Furthermore, Fig. 9 presents the strain field at the appearance of the first crack and at the end of the test. The failure mode of the samples shows that in all cases the crack started in the region between notches, but that, due to the restriction imposed by the fibers, there was a reorientation of the crack propagation. In addition to the reorientation of crack propagation, multiple cracks can be seen for specimens reinforced with 1.0% and 1.5% of PVA fiber. This multiple-cracking behavior is expected for composites with a high content of discrete fibers, as observed by [41].

4.4. Flexural strength

Fig. 10(a) shows the applied force, converted to an equivalent stress, as function of crack mouth opening displacement (CMOD) results of the three-point bending tests of the reference and PVA fiber reinforced cement paste. Furthermore, the summary of the data obtained in each test is shown in Table 8 considering the mean results and their respective standard deviations. The parameters in Table 8 were calculated according to the recommendations of the EN 14651 standard [49]: stress at the limit of proportionality (σ_{lop}) estimated as the maximum stress value in the range of CMOD up to 0.05 mm; maximum stress (σ_u) defined as the maximum stress value after the appearance of the first crack; residual stresses ($f_{r,i}$) calculated for pre-defined values of CMOD (0.5, 1.5, 2.5 and 3.5 mm) and also defined in Model Code 2010 [50]; toughness at 4 mm of CMOD ($T_{4.0}$) expressed by the total area of the load (kN) as function of CMOD (mm) curve.

In Fig. 10(a) it can be seen that the fibers contribute significantly to the maximum strength and residual capacity of the class G cement

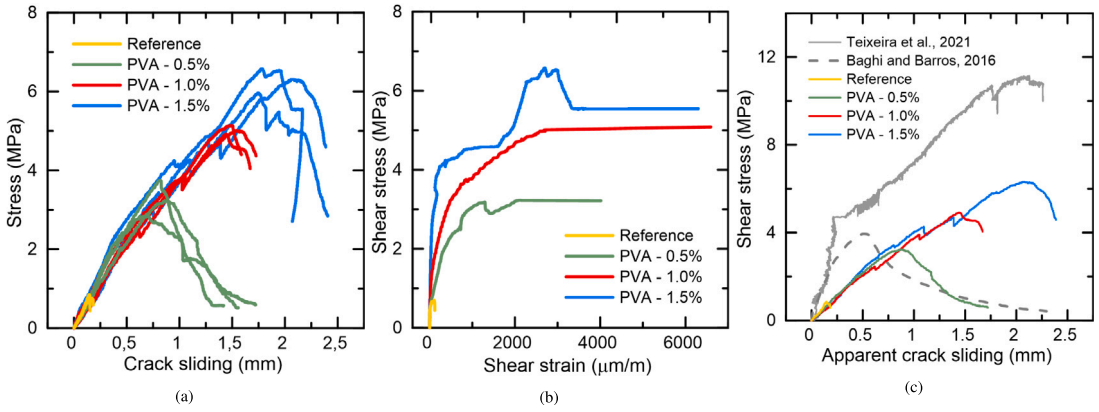

Fig. 8. Iosipescu shear test results showing shear stress as a function of (a) crack sliding, (b) shear strain, and (c) a comparison with literature curves [20,40].

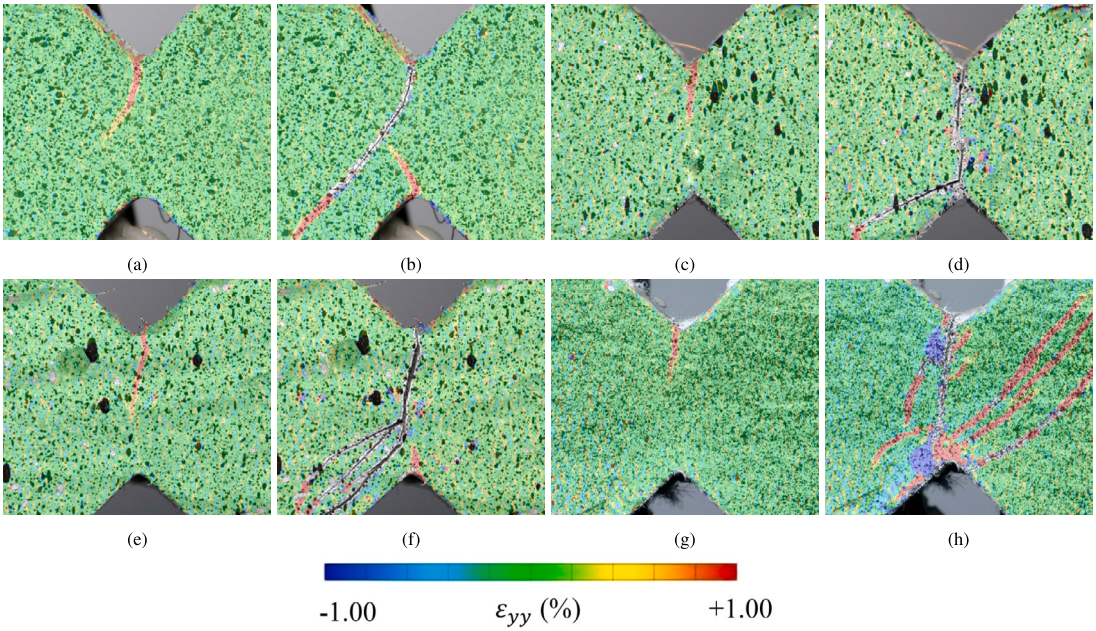

Fig. 9. The strain field at the appearance of the first crack and at the end of the test. (a) and (b) are the DIC images for the reference case, (c) and (d) for the mixture reinforced with 0.5% of PVA fiber, (e) and (f) for the mixture reinforced with 1.0% of PVA fiber, and (g) and (h) for the mixture reinforced with 1.5% of PVA fiber.

Table 7
Summarized composite properties by mechanical and DIC analysis from the Iosipescu shear tests.

Formulation	Max. load (kN)	Max. shear stress (MPa)	Apparent crack sliding (mm)	Crack opening at max. stress (mm)	Number of cracks at max. stress
Reference	0.14 ± 0.01	0.77 ± 0.08	0.14 ± 0.001	–	1
PVA-0.5%	0.59 ± 0.08	3.28 ± 0.43	0.79 ± 0.090	0.209	1
PVA-1.0%	0.90 ± 0.02	5.02 ± 0.11	1.49 ± 0.045	0.391	3
PVA-1.5%	1.13 ± 0.05	6.28 ± 0.31	1.86 ± 0.173	0.454	5

Table 8
Summarized composite properties by mechanical analysis under three-point bending load.

Mixture	P_{lop} (kN)	σ_{lop} (MPa)	P_u (kN)	σ_u (MPa)	$f_{r,1}$ (MPa)	$f_{r,2}$ (MPa)	$f_{r,3}$ (MPa)	$f_{r,4}$ (MPa)	$T_{4,0}$ (J)
Reference	0.55 (± 0.02)	3.45 (± 0.10)	-	-	-	-	-	-	-
PVA-0.5%	0.52 (± 0.01)	3.25 (± 0.07)	0.59 (± 0.03)	3.71 (± 0.17)	2.97 (± 0.15)	1.70 (± 0.12)	0.47 (± 0.02)	0.27 (± 0.03)	0.87 (± 0.03)
PVA-1.0%	0.57 (± 0.01)	3.54 (± 0.07)	1.15 (± 0.01)	(7.20 (± 0.08)	6.03 (± 0.66)	3.49 (± 0.31)	1.05 (± 0.21)	0.55 (± 0.09)	1.74 (± 0.10)
PVA-1.5%	0.72 (± 0.03)	4.51 (± 0.17)	1.40 (± 0.07)	8.73 (± 0.44)	6.94 (± 0.67)	6.97 (± 0.43)	3.86 (± 0.06)	2.71 (± 0.03)	3.24 (± 0.15)
PVA-1.0% (70 °C)	0.68 (± 0.02)	4.25 (± 0.12)	1.54 (± 0.14)	9.65 (± 0.90)	7.89 (± 0.24)	3.61 (± 1.41)	1.39 (± 0.79)	0.72 (± 0.34)	2.25 (± 0.39)

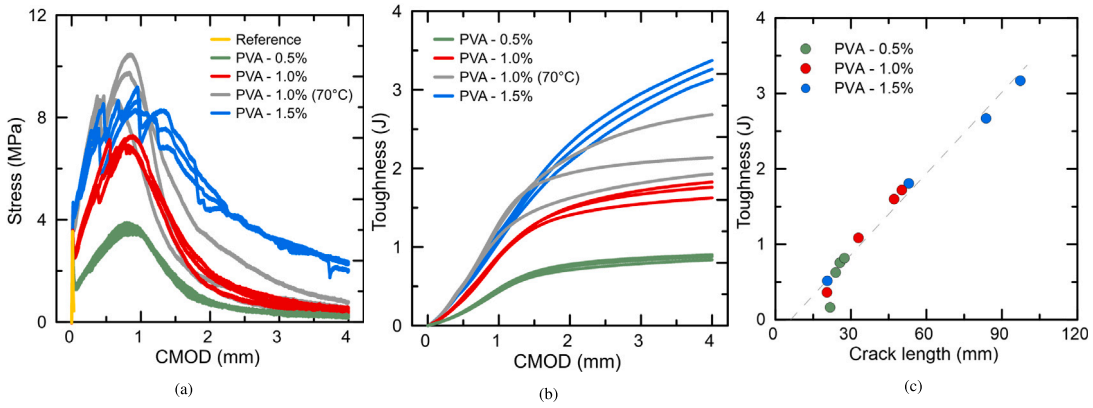

Fig. 10. Mechanical behavior of the flexural specimens plotted by crack mouth opening displacement (CMOD) (a), toughness as function of CMOD (b), and correlation between toughness and crack length from DIC measurements (c).

paste, resulting in maximum bending stress of up to 2.5 times greater than the reference specimens. In general, the fiber-reinforced samples showed residual stresses higher than the σ_{lop} up to 1 mm crack openings. However, as the PVA fibers used are only 6 mm long, after the 1 mm CMOD it is possible to observe a decrease in residual stresses for all composites evaluated. In the literature, it is possible to notice that for PVA, polyethylene, and steel fibers with a length of at least 12 mm, these residual stresses tend to remain constant after the appearance of the first crack, since the fibers continue to serve as a tension transfer bridge in the cracked zone to largest CMODs [6,44,51,52]. Furthermore, and as already observed by several authors, the residual stresses increase with increasing fiber content, since there will be more fibers in the cracked zone to control the crack propagation [6,18,44,53,54].

The material toughness plotted as function of CMOD is provided in Fig. 10(b), which translates the residual capacity of the material into energy absorption capacity. Composites with higher fiber content showed a greater ability to absorb energy with increasing CMOD, resulting in an approximately linear correlation between fiber increment and toughness at 4 mm CMOD ($T_{4.0} = 2.37 \cdot f_{\text{content}} - 0.42$, ($R^2 = 0.98$)). Furthermore, when correlating the crack length (CL) with the composite toughness (T) in the graph of Fig. 10(c), it is also possible to observe an approximately linear relationship between the parameters ($T = 0.0361 \cdot CL - 0.2422$, ($R^2 = 0.972$)). For this analysis, the toughness of all mixtures was collected for each pre-established CMOD (0.5, 1.5, 2.5, and 3.5 mm), and through DIC, it was possible to define the crack length for each CMOD. Therefore, the ability of the material to absorb energy is directly related to fiber content and crack length.

It was also possible to define the failure mode and the evolution behavior of the cracks from the DIC images (Fig. 11). While the PVA-0.5% specimens showed the development of a single crack with increasing CMOD, the PVA-1.0% and PVA-1.5% specimens resulted in multiple cracking behaviors in the notch region. This multiple cracking phenomenon occurs mainly when the energy needed to open a new crack becomes less than the energy to continue propagating an already open crack [9,10,55]. Therefore, it can be noted that for class G cement paste with PVA fiber content above 1.0%, the bridging strength of the fibers is at some points higher than the strength of the cement paste matrix.

Finally, and since the ultimate application we consider is fiber reinforcement of oil well cement, the curing temperature was considered as an analysis variable. As a preliminary assessment of downhole conditions on the mechanical properties of the cement paste, specimens were cured at 70 °C at atmospheric pressure. Figs. 10(a) and 10(b) show the stress and toughness as function of CMOD for the PVA-1.0% samples cured at elevated temperature. We observe that both σ_{lop} and σ_u increase with increasing curing temperature, indicating an acceleration in the cement paste hydration process and greater matrix strength at the time of testing. Since the decomposition of calcium hydroxide occurs at about 350 °C, and partial volatilization of calcium silicate hydrate gel commences at about 500 °C, it was not expected to have significant damage to the cement paste matrix under 70 °C curing temperature [56,57]. This observation is in agreement with «avdar [57], who found that a cement matrix reinforced with 1.0% PVA fiber improves its flexural strength for curing temperatures up to 100 °C. Additionally, Serafini et al. [22] affirms that the thermal energy can act as a catalyst for the topochemical reaction of anhydrous silicates deposited in the interfacial transition zone (ITZ). This statement is in line with recently published studies stating that for temperatures around 100 °C, the formation of new hydration products capable of filling the pores is favorable [58,59].

5. Summary and outlook

This study has considered effects of adding different concentrations of PVA fibers to a class G oil well cement paste. Fiber additives are generally considered to impart enhanced mechanical properties in cementitious materials, and to improve the load-carrying capacity of hardened cement. Our study has shown that the addition of fibers in the cement paste mixtures increased the strength of the material when subjected to shear loads, in addition to ensuring an increase in ductility. This increase in ductility was translated from the relationship between peak stress and apparent crack sliding. In the case of bending, the fiber contributed significantly to the maximum strength and residual capacity of the class G cement paste, resulting in maximum bending stress of up to 2.5 times more than the reference specimens. In direct compression tests, it was observed that the reference cement paste and the cement paste with 0.5% PVA fiber showed modest reinforcement by friction with increasing confinement, and this frictional reinforcing was more evident in the reinforced specimen. Moreover, the fiber addition did not influence the linear elastic behavior of the cement paste specimens, nor the maximum deviatoric stress level. While the presence of fibers resulted in increased effective viscosity of all tested cement pastes, the most significant impact of fiber additive to cement paste was found to be an improved ability to arrest tensile crack growth and to absorb energy when evaluating tensile and shear loads. These properties can make PVA fibers an attractive additive in cases where well cements are likely to be subjected to tensile loading, or as a possible additive for flexible expanding cement systems, [60].

Additional research related to fiber additions to oil well cement paste could target higher confining pressures than considered in this study to further explore the frictional strengthening of the hardened cement, and the combined impacts of temperature and pressure on the performance of the cement. Our current study is also limited to moulded cement specimens, and not cement hardened inside a casing or in the annular space between casings. It is likely that the presence of

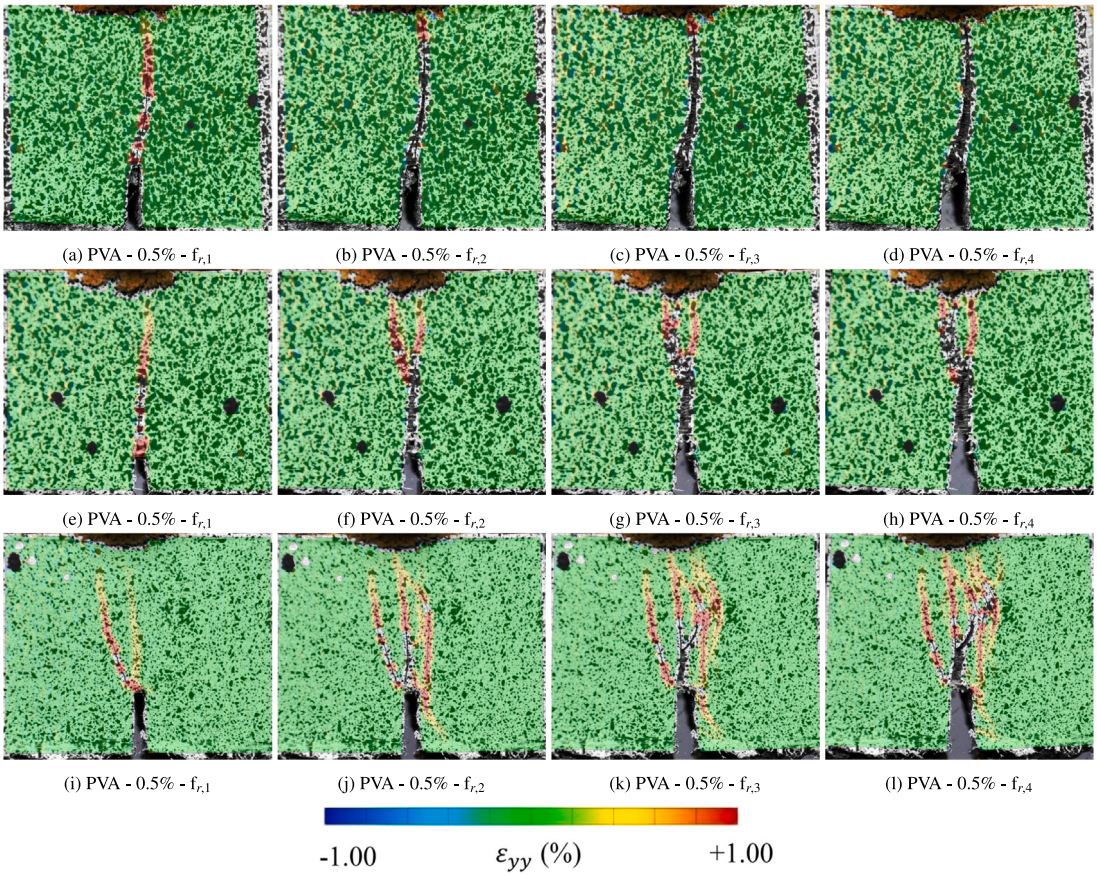

Fig. 11. The strain field referring to the pre-established residual stresses ($f_{r,1}$, $f_{r,2}$, $f_{r,3}$ and $f_{r,4}$). (a)–(d) are the DIC images for the mixture reinforced with 0.5% PVA fiber, (e)–(h) for the mixture reinforced with 1.0% PVA fiber, and (i)–(l) for the mixture reinforced with 1.5% PVA fiber.

casing or formation walls, and shear-induced migration [61,62] during cementing may impact fiber distribution within the cement paste. A consequence may be fiber-depleted wall layers adjacent to the casing or wellbore walls, or along the narrow side of an eccentric annulus. Future studies should examine fiber particle distribution and orientation within cement plugs and annular cement sheaths and its impact on the performance of the hardened cement. Finally, the longevity and fiber particles in a downhole environment should also be assessed.

CRediT authorship contribution statement

Victor Nogueira Lima: Conceptualization, Methodology, Investigation, Writing – original draft. **Hans Joakim Skadsem:** Supervision, Writing – original draft. **Katherine Beltrán-Jiménez:** Methodology, Investigation. **Raquel Quadros Velloso:** Resources, Supervision. **Flávio de Andrade Silva:** Resources, Supervision.

Declaration of competing interest

The authors declare that they have no known competing financial interests or personal relationships that could have appeared to influence the work reported in this paper.

Data availability

Data will be made available on request.

Acknowledgments

This study was financed in part by the Coordenação de Aperfeiçoamento de Pessoal de Nível Superior – Brasil (CAPES) – Finance Code 001, by Brazilian funding agencies FAPERJ and CNPq, by Lafarge Holcim, with the donation of class G cement, by BASF, Germany, with the donation of the defoamer, and by Kuraray, with the donation of the Kuraray Poval™ additive and PVA fiber. This research is a cooperation between PUC-Rio, NORCE Norwegian Research Centre AS, and the University of Stavanger, and partly funded by the Research Council of Norway (RCN) under the BRANOR Project (309295).

References

[1] E.B. Nelson, D. Guillot, Well Cementing, Vol. 2, Newnes, Sugar Land, Texas, USA, 2006.
[2] V.C. Li, On engineered cementitious composites (ECC) a review of the material and its applications, J. Adv. Concr. Technol. 1 (3) (2003) 215–230, http://dx.doi.org/10.3151/JACT.1.215.
[3] Q. Jin, V.C. Li, Development of lightweight engineered cementitious composite for durability enhancement of tall concrete wind towers, Cem. Concr. Compos. 96 (2019) 87–94, http://dx.doi.org/10.1016/J.CEMCONCOMP.2018.11.016.
[4] C.G. Cho, A.J. Kappos, H.J. Moon, H.J. Lim, Experiments and failure analysis of SHCC and reinforced concrete composite slabs, Eng. Fail. Anal. 56 (2015) 320–331, http://dx.doi.org/10.1016/J.ENGFAILANAL.2015.01.009.
[5] H.D. Yun, Flexural behavior and crack-damage mitigation of plain concrete beam with a strain-hardening cement composite (SHCC) layer at tensile region, Composites B 45 (1) (2013) 377–387, http://dx.doi.org/10.1016/J.COMPOSITESB.2012.05.053.
[6] W.G. Bareiro, F. de Andrade Silva, E.D. Sotelino, Thermo-mechanical behavior of stainless steel fiber reinforced refractory concrete: Experimental and numerical analysis, Constr. Build. Mater. 240 (2020) 117881, http://dx.doi.org/10.1016/J.CONBUILDMAT.2019.117881.

[7] A. Wang, S. Cao, E. Yilmaz, Influence of types and contents of nano cellulose materials as reinforcement on stability performance of cementitious tailings backfill, Constr. Build. Mater. 344 (2022) 128179, http://dx.doi.org/10.1016/j.conbuildmat.2022.128179.

[8] G.P. Van Zijl, F.H. Wittmann, B.H. Oh, P. Kabele, R.D. Toledo Filho, E.M. Fairbairn, V. Slowik, A. Ogawa, H. Hoshiro, V. Mechtcherine, F. Altmann, M.D. Lepech, Durability of strain-hardening cement-based composites (SHCC), Mater. Struct./Materiaux Et Constr. 45 (10) (2012) 1447–1463, http://dx.doi.org/10.1617/S11527-012-9845-Y/FIGURES/9, https://link.springer.com/article/10.1617/s11527-012-9845-y.

[9] V. Mechtcherine, Novel cement-based composites for the strengthening and repair of concrete structures, Constr. Build. Mater. 41 (2013) 365–373, http://dx.doi.org/10.1016/J.CONBUILDMAT.2012.11.117.

[10] I. Curosu, V. Mechtcherine, D. Forni, E. Cadoni, Performance of various strain-hardening cement-based composites (SHCC) subject to uniaxial impact tensile loading, Cem. Concr. Res. 102 (2017) 16–28, http://dx.doi.org/10.1016/J.CEMCONRES.2017.08.008.

[11] P. Jun, V. Mechtcherine, Behaviour of strain-hardening cement-based composites (SHCC) under monotonic and cyclic tensile loading: Part 1 – experimental investigations, Cem. Concr. Compos. 32 (10) (2010) 801–809, http://dx.doi.org/10.1016/J.CEMCONCOMP.2010.07.019.

[12] V. Mechtcherine, F.D.A. Silva, S. Müller, P. Jun, R.D.T. Filho, Coupled strain rate and temperature effects on the tensile behavior of strain-hardening cement-based composites (SHCC) with PVA fibers, Cem. Concr. Res. 42 (11) (2012) 1417–1427, http://dx.doi.org/10.1016/J.CEMCONRES.2012.08.011.

[13] A. Wang, S. Cao, E. Yilmaz, Effect of height to diameter ratio on dynamic characteristics of cemented tailings backfills with fiber reinforcement through impact loading, Constr. Build. Mater. 322 (2022) 126448, http://dx.doi.org/10.1016/j.conbuildmat.2022.126448.

[14] L. Li, V.C. Boncan, A. Brandl, A.K. Jordan, Fundamental investigation of mechanical properties of additives and class H cement under downhole conditions, 2015, http://dx.doi.org/10.2118/176175-MS.

[15] L. Li, M. Kellum, A. Doan, In-situ tensile strength testing: Awareness of variations with testing environment, 2016, http://dx.doi.org/10.2118/180347-MS.

[16] C. Soranakom, B. Mobasher, Correlation of tensile and flexural responses of strain softening and strain hardening cement composites, Cem. Concr. Compos. 30 (6) (2008) 465–477, http://dx.doi.org/10.1016/j.cemconcomp.2008.01.007, https://www.engineeringvillage.com/share/document.url?mid=cpx_30c22111a019cf2c5M769120613775538database=cpx.

[17] B. Li, L. Xu, Y. Shi, Y. Chi, Q. Liu, C. Li, Effects of fiber type, volume fraction and aspect ratio on the flexural and acoustic emission behaviors of steel fiber reinforced concrete, Constr. Build. Mater. 181 (2018) 474–486, http://dx.doi.org/10.1016/J.CONBUILDMAT.2018.06.065, https://www.sciencedirect.com/science/article/pii/S0950061818314557.

[18] V.N. Lima, D.C.T. Cardoso, F. d. A. Silva, Creep mechanisms in pre-cracked polypropylene and steel fiber–reinforced concrete, J. Mater. Civ. Eng. 33 (8) (2021) 04021187, http://dx.doi.org/10.1061/(ASCE)MT.1943-5533.0003775, https://ascelibrary.org/doi/abs/10.1061/%28ASCE%29MT.1943-5533.0003775.

[19] G.P. van Zijl, Improved mechanical performance: Shear behaviour of strain-hardening cement-based composites (SHCC), Cem. Concr. Res. 37 (8) (2007) 1241–1247, http://dx.doi.org/10.1016/J.CEMCONRES.2007.04.009.

[20] H. Baghi, J.A.O. Barros, Shear properties of the strain hardening cementitious composite material, J. Mater. Civ. Eng. 28 (10) (2016) 04016093, http://dx.doi.org/10.1061/(ASCE)MT.1943-5533.0001603, https://ascelibrary.org/doi/abs/10.1061/%28ASCE%29MT.1943-5533.0001603.

[21] Y. Yang, Y. Deng, Mechanical properties of hybrid short fibers reinforced oil well cement by polyester fiber and calcium carbonate whisker, Constr. Build. Mater. 182 (2018) 258–272, http://dx.doi.org/10.1016/J.CONBUILDMAT.2018.06.110.

[22] R. Serafini, R.R. Agra, L.A. Bitencourt, A. de la Fuente, A.D. de Figueiredo, Bond–slip response of steel fibers after exposure to elevated temperatures: Experimental program and design-oriented constitutive equation, Compos. Struct. 255 (2021) 112916, http://dx.doi.org/10.1016/J.COMPSTRUCT.2020.112916.

[23] L. Li, D. Gao, Z. Li, M. Cao, J. Gao, Z. Zhang, Effect of high temperature on morphologies of fibers and mechanical properties of multi-scale fiber reinforced cement-based composites, Constr. Build. Mater. 261 (2020) 120487, http://dx.doi.org/10.1016/J.CONBUILDMAT.2020.120487.

[24] Q. Li, X. Gao, S. Xu, Y. Peng, Y. Fu, Microstructure and mechanical properties of high-toughness fiber-reinforced cementitious composites after exposure to elevated temperatures, J. Mater. Civ. Eng. 28 (11) (2016) 04016132, http://dx.doi.org/10.1061/(ASCE)MT.1943-5533.0001647, https://ascelibrary.org/doi/abs/10.1061/%28ASCE%29MT.1943-5533.0001647 https://ascelibrary.org/doi/10.1061/.

[25] Q. Du, J. Wei, J. Lv, Effects of high temperature on mechanical properties of polyvinyl alcohol engineered cementitious composites (PVA-ecc), Int. J. Civ. Eng. 16 (8) (2018) 965–972, http://dx.doi.org/10.1007/S40999-017-0245-0/FIGURES/7, https://link.springer.com/article/10.1007/s40999-017-0245-0.

[26] M.D.S. Magalhães, R.D. Toledo Filho, E.D.M.R. Fairbairn, Thermal stability of PVA fiber strain hardening cement-based composites, Constr. Build. Mater. 94 (2015) 437–447, http://dx.doi.org/10.1016/J.CONBUILDMAT.2015.07.039.

[27] C.J.S. Petrie, The rheology of fibre suspensions, J. Non-Newton. Fluid Mech. 87 (2) (1999) 369–402, http://dx.doi.org/10.1016/S0377-0257(99)00069-5.

[28] L. Martinie, P. Rossi, N. Roussel, Rheology of fiber reinforced cementitious materials: Classification and prediction, Cem. Concr. Res. 40 (2) (2010) 226–234, http://dx.doi.org/10.1016/j.cemconres.2009.08.032, https://linkinghub.elsevier.com/retrieve/pii/S0008884609002518.

[29] R.M. Ahmed, N.E. Takach, Fiber sweeps for hole cleaning, SPE Drill. Complet. 24 (04) (2009) 564–573, http://dx.doi.org/10.2118/113746-PA, SPE-113746-PA.

[30] API, API 10A: Specification for cements and materials for well cementing, 2011.

[31] API, 10B-2: Recommended practice for testing well cements, 2013.

[32] I. Curosu, V. Mechtcherine, O. Millon, Effect of fiber properties and matrix composition on the tensile behavior of strain-hardening cement-based composites (SHCCs) subject to impact loading, Cem. Concr. Res. 82 (2016) 23–35, http://dx.doi.org/10.1016/J.CEMCONRES.2015.12.008.

[33] J. Yu, Y. Chen, C.K. Leung, Micromechanical modeling of crack-bridging relations of hybrid-fiber strain-hardening cementitious composites considering interaction between different fibers, Constr. Build. Mater. 182 (2018) 629–636, http://dx.doi.org/10.1016/J.CONBUILDMAT.2018.06.115.

[34] E.H. Yang, S. Wang, Y. Yang, V.C. Li, Fiber-bridging constitutive law of engineered cementitious composites, J. Adv. Concr. Technol. 6 (1) (2008) 181–193, http://dx.doi.org/10.3151/JACT.6.181.

[35] É. Lac, A. Parry, Non-Newtonian end-effects in standard oilfield rheometers, J. Rheol. 61 (4) (2017) 833, http://dx.doi.org/10.1122/1.4986925, https://sor.scitation.org/doi/abs/10.1122/1.4986925.

[36] H.J. Skadsem, A. Saasen, Concentric cylinder viscometer flows of herschel-bulkley fluids, Appl. Rheol. 29 (1) (2019) 173–181, http://dx.doi.org/10.1515/ARH-2019-0015/MACHINEREADABLECITATION/RIS, https://www.degruyter.com/document/doi/10.1515/arh-2019-0015/html.

[37] V.N. Lima, F. d.A. Silva, H.J. Skadsem, K. Beltrán-Jiménez, J.K. Sunde, Effects of confinement pressure on the mechanical behavior of an oil well cement paste, J. Pet. Sci. Eng. 208 (2022) 109769, http://dx.doi.org/10.1016/J.PETROL.2021.109769.

[38] R. Lorenzoni, V.N. Lima, T.C.S. Figueiredo, M. Hering, S. Paciornik, M. Curbach, V. Mechtcherine, F. de Andrade Silva, Macro and meso analysis of cement-based materials subjected to triaxial and uniaxial loading using X-ray microtomography and digital volume correlation, Constr. Build. Mater. 323 (2022) 126558, http://dx.doi.org/10.1016/J.CONBUILDMAT.2022.126558, https://linkinghub.elsevier.com/retrieve/pii/S0950061822002501.

[39] ASTM, ASTM D5379/D5379M-12: Standard test method for shear properties of composite materials by the V-notched beam method, 2014, http://dx.doi.org/10.1520/D5379.

[40] F.P. Teixeira, D.C.T. Cardoso, F. de Andrade Silva, On the shear behavior of natural curauá fabric reinforced cement-based composite systems, Eng. Struct. 246 (2021) 113054, http://dx.doi.org/10.1016/J.ENGSTRUCT.2021.113054.

[41] R. Lorenzoni, M. Tinoco, S. Paciornik, F. de Andrade Silva, The use of X-ray microtomography to investigate the shear behavior of hybrid fiber reinforced strain hardening cementitious composites, J. Build. Eng. 43 (2021) 103126, http://dx.doi.org/10.1016/J.JOBE.2021.103126.

[42] H.A. Bruck, S.R. McNeill, M.A. Sutton, W.H. Peters, Digital image correlation using Newton–Raphson method of partial differential correction, Exp. Mech. 29 (3) (1989) 261–267, http://dx.doi.org/10.1007/BF02321405, https://link.springer.com/article/10.1007/BF02321405.

[43] M. Sutton, W. Wolters, W. Peters, W. Ranson, S. McNeill, Determination of displacements using an improved digital correlation method, Image Vis. Comput. 1 (3) (1983) 133–139, http://dx.doi.org/10.1016/0262-8856(83)90064-1.

[44] M.P. Tinoco, F. d.A. Silva, On the mechanical behavior of hybrid fiber reinforced strain hardening cementitious composites subjected to monotonic and cyclic loading, J. Mater. Res. Technol. 11 (2021) 754–768, http://dx.doi.org/10.1016/J.JMRT.2021.01.053.

[45] J. Handin, Strength of oil well cements at downhole pressure-temperature conditions, SPE J. 5 (04) (1965) 341–347, http://dx.doi.org/10.2118/1300-PA.

[46] Y. Sakai, M. Nakatani, A. Takeuchi, Y. Omorai, T. Kishii, Mechanical behavior of cement paste and alterations of hydrates under high-pressure triaxial testing, J. Adv. Concr. Technol. 14 (1) (2016) 1–12, http://dx.doi.org/10.3151/jact.14.1.

[47] Y. Li, Y. Lu, R. Ahmed, B. Han, Y. Jin, Nonlinear stress-strain model for confined well cement, 2019, http://dx.doi.org/10.3390/ma12162626.

[48] V.C. Li, S. Wang, C. Wu, Tensile strain-hardening behavior of polyvinyl alcohol engineered cementitious composite (PVA-ECC), Mater. J. 98 (6) (2001) 483–492, http://dx.doi.org/10.14359/10851.

[49] European Standard, EN 14651: Test method for metallic fibered concrete - measuring the flexural tensile strength (limit of proportionality (LOP), residual), 2005.

[50] Fib, Fib model code, 2010, http://dx.doi.org/10.1002/9783433604090, Switzerland.

[51] S. Sasmal, G. Avinash, Investigations on mechanical performance of cementitious composites micro-engineered with poly vinyl alcohol fibers, Constr. Build. Mater. 128 (2016) 136–147, http://dx.doi.org/10.1016/J.CONBUILDMAT.2016.10.025.

[52] Y. Zhou, B. Xi, K. Yu, L. Sui, F. Xing, Mechanical properties of hybrid ultra-high performance engineered cementitous composites incorporating steel and polyethylene fibers, Materials 11 (8) (2018) 1448, http://dx.doi.org/10.3390/MA11081448, https://www.mdpi.com/1996-1944/11/8/1448/htm https://www.mdpi.com/1996-1944/11/8/1448.

[53] J.-H. Lee, B. Cho, E. Choi, Flexural capacity of fiber reinforced concrete with a consideration of concrete strength and fiber content, Constr. Build. Mater. 138 (2017) 222–231, http://dx.doi.org/10.1016/J.CONBUILDMAT.2017.01.096, https://www.sciencedirect.com/science/article/pii/S0950061817301393.

[54] V.M. de Alencar Monteiro, L.R. Lima, F. de Andrade Silva, On the mechanical behavior of polypropylene, steel and hybrid fiber reinforced self-consolidating concrete, Constr. Build. Mater. 188 (2018) 280–291, http://dx.doi.org/10.1016/j.conbuildmat.2018.08.103.

[55] V.C. Li, Tailoring ECC for special attributes: A review, Int. J. Concrete Struct. Mater. 6 (3) (2012) 135–144, http://dx.doi.org/10.1007/S40069-012-0018-8/FIGURES/16, https://ijcsm.springeropen.com/articles/10.1007/s40069-012-0018-8.

[56] E. Gallucci, X. Zhang, K.L. Scrivener, Effect of temperature on the microstructure of calcium silicate hydrate (C-S-H), Cem. Concr. Res. 53 (2013) 185–195, http://dx.doi.org/10.1016/J.CEMCONRES.2013.06.008.

[57] A. Çavdar, A study on the effects of high temperature on mechanical properties of fiber reinforced cementitious composites, Composites B 43 (5) (2012) 2452–2463, http://dx.doi.org/10.1016/J.COMPOSITESB.2011.10.005.

[58] K.Y. Kim, T.S. Yun, K.P. Park, Evaluation of pore structures and cracking in cement paste exposed to elevated temperatures by X-ray computed tomography, Cem. Concr. Res. 50 (2013) 34–40, http://dx.doi.org/10.1016/J.CEMCONRES.2013.03.020.

[59] M.C. Farage, J. Sercombe, C. Gallé, Rehydration and microstructure of cement paste after heating at temperatures up to 300 °C, Cem. Concr. Res. 33 (7) (2003) 1047–1056, http://dx.doi.org/10.1016/S0008-8846(03)00005-X.

[60] S. Le Roy-Delage, C. Baumgarte, M. Thiercelin, B. Vidick, New cement systems for durable zonal isolation, 2000, http://dx.doi.org/10.2118/59132-MS.

[61] L.A. Mondy, H. Brenner, S.A. Altobelli, J.R. Abbott, A.L. Graham, Shear-induced particle migration in suspensions of rods, J. Rheol. 38 (2) (1994) 444–452, http://dx.doi.org/10.1122/1.550522.

[62] S. Strednak, S. Shaikh, J.E. Butler, E. Guazzelli, Shear-induced migration and orientation of rigid fibers in an oscillatory pipe flow, Phys. Rev. Fluids 3 (2018) 091301, http://dx.doi.org/10.1103/PhysRevFluids.3.091301.